Available online at www.sciencedirect.com
SCIENCE DIRECT
Carbon 44 (2006) 954–961
CARBON
www.elsevier.com/locate/carbon

Pore structures in shungites as revealed by small-angle neutron scattering

M.V. Avdeev [a,*], T.V. Tropin [a], V.L. Aksenov [a], L. Rosta [b], V.M. Garamus [c], N.N. Rozhkova [d]

[a] Joint Institute for Nuclear Research, Joliot-Curie Str. 6, 141980 Dubna, Russian Federation
[b] Research Institute for Solid State Physics and Optics, Budapest, Hungary
[c] GKSS Research Center, Geesthacht, Germany
[d] Institute of Geology, Karelian Research Centre RAS, Petrozavodsk, Russia

Received 18 May 2005; accepted 10 October 2005
Available online 21 November 2005

Abstract

The analysis of the small-angle neutron scattering data from shungites, one of the natural forms of carbon, is reported. Samples from different deposits are investigated. It is shown that shungites have a complex pore structure at a nanoscale of 1–100 nm depending on their origin. Along with it, common features, in particular, two-level organization at the given scale can be observed. The absorption of deuterated water by shungites is used to match the scattering from open pores and to separate the information about the open and closed porosity in the samples. The revealed structural units are compared with the previous experimental results obtained by the complementary techniques.

Keywords: Shungite; Microstructure; Microporosity; Particle size

1. Introduction

Shungites are carbon-rich rocks of Precambrian age widespread over Russian Karelia [1]. In recent years shungites have been attracting much attention due to the prospects of their various industrial and biomedical applications. Thus, this carbon acts as an efficient catalyst of hydrogenation at low temperatures [2], an adsorbent and filter in water purification processes [3] and multi-functional filler of polymeric and inorganic binders [4,5]. It can be used [6] as the basic radiation screening constituent of construction materials. In addition, shungite carbon can efficiently replace coke and quartzite to remove liquid slag in metallurgy and in electro thermal processes in the production of various alloys and ceramics [7]. A special attention to shungites is connected with the reported [8] presence of fullerenes in them. Also, the possibility to disperse shungites into aqueous medium [9] in the same way as in the synthesis of fullerene dispersions [10] should be mentioned.

A general task of the study of shungites is to find out the most effective technologies of their treatment and application. In this connection, the knowledge about the structure of these rocks and its modifications is of great importance. Shungite carbon is characterized as metastable and non-graphitized. On the basis of the data of different techniques including chemical analysis and chromatography, electron and X-ray diffraction, high-resolution transmission electron microscopy (HRTEM), atomic-force microscopy (AFM) and small-angle X-ray scattering (SAXS), it has been assumed [11–16] that the structure of shungite is a set of packed globular or ellipsoidal multi-layered units

* Corresponding author. Tel.: +7 096 21 62 674; fax: +7 096 21 65 484.
E-mail address: avd@nf.jinr.ru (M.V. Avdeev).

0008-6223/$ - see front matter © 2005 Elsevier Ltd. All rights reserved.
doi:10.1016/j.carbon.2005.10.010

with a size of less than 10 nm aggregated into formations up to order of 1 μm. Different structural units at a nanoscale of 1–100 nm have been detected. Despite the structural similarity, shungites from various deposits differ in bulk morphology and offer a wide range of useful properties such as porosity and surface area.

In the present paper we use the small-angle neutron scattering (SANS) to reveal structural features of shungite powders at the scale of 1–100 nm complementary to the previous investigations. One aim of the current work is to compare the SANS signals from shungites of different deposits and to determine characteristic parameters of various types of the structural organization of shungites. Another aim is to use the contrast variation technique in the SANS experiments in view of the fact that the scattering length densities of carbon ($\rho \sim 7 \times 10^{10}\,\mathrm{cm}^{-2}$) and heavy water ($\rho \sim 6.34 \times 10^{10}\,\mathrm{cm}^{-2}$) are close. Following changes in the neutron scattering from the powders after they have absorbed heavy water, we separate effects of the closed and open porosity on the scattering and conclude about the pore structures in shungites.

Shungites from three deposits of Shunga, Maksovo and Chebolaksha are investigated. The samples were chosen from the deposits known to be of the same age but under different regional conditions (temperature, pressure and hydrothermal regime). From the point of view of the geological concepts [1,17] all shungites were formed through the single mechanism while their structural modifications as a result of various environmental conditions took place. Thus, the Maksovo shungite was under hydrothermal influence according to geological evidences such as carbonaceous breccias [1] and can be regarded as a modification of the Shunga shungite [17,25] with an increase in its open porosity and surface area. The later is supported by the close location of the two deposits and similar physical chemical properties of both shungites after the activation performed in laboratory conditions (up to two hours at 1100 K under flowing steam and flowing steam with CO_2). The Chebolaksha shungite is distinguished among three samples, according to the geological data, by the higher pressure conditions.

2. Experiment and data treatment

Shungite powders with an average particle size of less than 40 μm were prepared by dry grinding of carbon-rich shungite rocks type-I sampled manually. Basic parameters of the powders are given in Table 1. Surface area given in Table 1 was measured by nitrogen adsorption according to the BET method and standard ASTM D 4820.

SANS experiments were carried out on the YuMO small-angle time-of-flight diffractometer at the IBR-2 pulsed reactor, Joint Institute for Nuclear Research, Dubna, Russia; on the Yellow Submarine small-angle instrument of the steady-state reactor of the Budapest Neutron Center (BNC), Hungary, and the SANS-1 small-angle instrument at the FRG-1 steady-state reactor of the GKSS Research Center, Geesthacht, Germany. The differential cross-section per sample volume (scattering intensity) isotropic over the radial angle φ on the detector was obtained as a function of the module of momentum transfer, $q = (4\pi/\lambda)\sin(\theta/2)$, where λ is the incident neutron wavelength and θ is the scattering angle. On the YuMO diffractometer [18,19] the neutron wavelengths within an interval of 0.05–0.5 nm and the sample–detector distances (SD) of 4 and 16 m (detector size 45 cm) were used to obtain scattering curves in a q-range of 0.08–5 nm^{-1}. The wavelength of the scattered neutrons registered by the detector was determined according to the time-of-flight method. The calibration procedure was made using vanadium [18]. At the BNC the fixed wavelengths of 0.45 and 1.2 nm (monochromatization $\Delta\lambda/\lambda = 13\%$) and sample–detector distances of 2 and 5.5 m (detector size 64 cm) were used to cover q-interval of 0.08–4 nm^{-1}. A standard procedure to calibrate curves on water [20] after the background and container corrections was performed. For calibration of the curves obtained at a neutron wavelength of 1.2 nm and SD of 5.5 m, the overlap of the data with those obtained at the same SD and wavelength of 0.45 nm was used. On the SANS-1 instrument [21] measurements were carried out at a neutron wavelength of 0.81 nm (monochromatization $\Delta\lambda/\lambda = 10\%$) and a series of sample–detector distances within the interval of 1–9 m (detector size 55 cm) to cover a q-range 0.04-2 nm^{-1}. As in the previous case, H_2O was used to calibrate the curves. At large sample–detector distances (>4.5 m) the calibrated curves were obtained by the recalculation of the curves for H_2O obtained at SD of 4 m with the corresponding distance coefficient. To check out the results of different corrections and calibration procedures, for several samples the scattering curves were obtained at all three setups and show complete reproducibility in overlapping q-regions.

Table 1
Basic characteristics of the studied samples [2,14,15]

Deposit	Inner surface area (BET) (m^2/g)	Open/closed porosity (%)	Average size of nanopores (SAXS) (nm)	Micro-porosity (%)
Shunga	2–5	4.7/ 8.1	2–4	67
Maksovo	180–240	18.8/6.6	3	96
Chebolaksha	5–10	1.6/12.4	6	–

Closed porosity (CPor) was determined through picnometric (ρ_{pic}) and X-ray ($\rho_{X\text{-}ray}$) densities as $\mathrm{CPor} = (1 - \rho_{pic}/\rho_{X\text{-}ray})\ 100\%$. The ρ_{pic} value was measured in kerosene. Total porosity (TPor) was determined from mercury porosimetry measurements (ρ_{part}) as $\mathrm{TPor} = (1 - \rho_{part}/\rho_{X\text{-}ray})\ 100\%$. Open porosity was obtained as a difference TPor − CPor. Microporosity was detected due to the comparison of surface area measured by nitrogen (sectional area of nitrogen molecule is $w = 0.16\ \mathrm{nm}^2$) and Rhodamine C ($w = 0.85\ \mathrm{nm}^2$).

Quartz plane cuvettes were filled with shungite powders. The bulk mass density of the samples, ρ_m, was determined from measurements of their mass and filled volume. The scattering from an empty cuvette was subtracted from the powder scattering as a background. To reveal a possible effect of multiple scattering the same powders were measured in the cuvettes of various thickness (1, 1.5 and 2 mm). No significant dependence of the scattering on the sample thickness was observed, which means that the multiple scattering effect can be neglected. For the contrast variation experiments heavy water (D_2O) was added to the powders from Maksovo and Shunga deposits in the same cuvettes, and the samples were left for one week and more. During the first two days one could observe how the boundary of moistening was moving to the bottom of the cuvettes. The changes in the scattering were followed during two weeks. After the first week of the absorption no significant changes in the scattering curves were observed, which allowed us to conclude that the adsorption stops and all open pores acceptable for the water are filled.

Several approaches given below were used to treat the scattering curves. Two regimes of the scattering intensity, $I(q)$, at different length scales were detected in the SANS experiments. Conditionally, we shall further refer to the detected levels as level I (small q-values) and II (large q-values). They were both fitted by the power law:

$$I(q) = B(1/q)^P + C, \tag{1}$$

where B is the parameter which contains information about the particle number density, n, volume, V, and scattering length density, ρ, of the scattering units; C is the background remaining after corrections. The value of the P exponent reflects the inner structure of the scattering units and characterizes [22] the type of their mass or surface organization according to the following classification:

$1 < P < 3$,
mass fractal with fractal dimension $D = P$; (2a)

$3 < P < 4$,
surface fractal with fractal dimension $D_S = 6 - P$; (2b)

$4 < P < 6$,
diffusive surface with exponent $\beta = (P - 4)/2$. (2c)

The case when $P = 4$ corresponds to the sharp smooth surface (Porod law), so that its dimension $D_S = 2$. A deviation from the power law (1) when q decreases reflects the so-called finite size effect. In this case the characteristic radius (radius of gyration), R, of the scattering particles at the given level can be estimated from the q-value corresponding to the place where the power law starts to break down. According to the expression connecting the direct and reciprocal spaces:

$$R \sim 2\pi/q. \tag{3}$$

At sufficiently low q-values, for a given scattering level the Guinier law should work. However, the pronounced behavior corresponding to this regime was detected only for level II in one sample (Maskovo). Level II in this case was treated in the frame of the unified exponential/power-law approach [23]. A general expression for one-scale level takes the form:

$$I(q) = G\exp(-q^2R^2/3) + B(1/q^*)^P + C, \tag{4}$$

where, in addition to Eq. (1), R is the radius of gyration of the scattering units corresponding to the given scattering level; $q^* = q/[\mathrm{erf}(qkR/6^{1/2})]^3$, where k is an empirical constant (1.6 for mass and 1.1 for surface scattering, respectively); and parameter G takes the form in monodisperse approximation:

$$G = nV^2(\rho - \bar{\rho})^2, \tag{5}$$

where $\bar{\rho}$ is the mean scattering length density of the bulk medium where the scattering units are located. The generalization of Eq. (4), which takes the scattering level I into account, is possible. In this case it is supposed that the scattering units form other larger particles, which produce the scattering corresponding to level I so that the whole scattering intensity can be presented as

$$I(q) = G_I\exp(-q^2R_I^2/3) + B_I\exp(-q^2R_{II}^2/3)(1/q_I*)^{P_I} + G_{II}\exp(-q^2R_{II}^2/3) + B_{II}(1/q_{II}*)^{P_{II}} + C, \tag{6}$$

where the I- and II-indexes correspond to the scattering units of levels I and II, respectively. It is important to note the presence in the second term of Eq. (6) of the exponential factor, $\exp(-q^2R_{II}^2/3)$, reflecting the scattering from units at level II. This factor makes it possible to distinguish two-level complex particles from the situation when two different types of particles scatter independently. In the latter case the resulting scattering intensity is just a sum of the corresponding Equations of type (4):

$$I(q) = G_I\exp(-q^2R_I^2/3) + B_I(1/q_I^*)^{P_I} + G_{II}\exp(-q^2R_{II}^2/3) + B_{II}(1/q_{II}^*)^{P_{II}} + C. \tag{7}$$

Another important feature of the treatment is that in all cases the finite size effect for level I is not observed in the obtained scattering curves, so the term $G_I\exp(-q^2R_I^2/3)$ was excluded from the final expressions. Below, to fit modified Eqs. (6), (7) to the scattering curves several steps were made. First, the values of the power-law terms were estimated with (1) in the corresponding q-intervals. Then, these values were fixed and other parameters in (6) and (7) were varied during fitting. After such estimates, best fits were found varying all parameters.

3. Results and discussion

SANS data normalized on the sample bulk mass density for the studied shungites are given in Fig. 1. The SANS curves coincide well with the previously obtained SAXS curves [15] in the region of the overlap of both techniques (comparison is given in Fig. 2). As one can see in Fig. 1, the scattering reflects a complex structural organization of

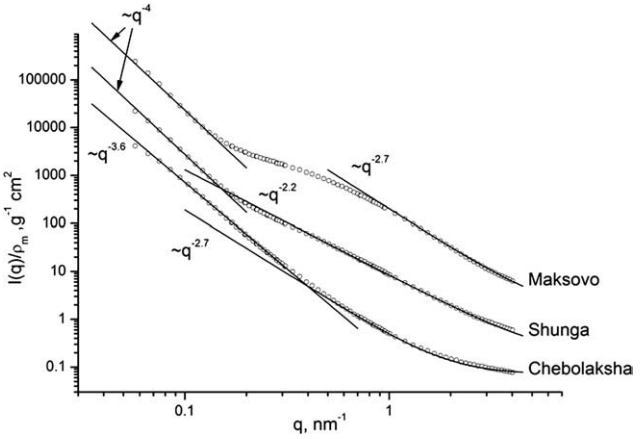

Fig. 1. Experimental SANS curves divided by the sample bulk density (points) and fits of power law (1) at different scales (solid lines). For convenient view the curves are multiplied by 100 (Maksovo) and 10 (Shunga). Statistical experimental errors are within the size of points.

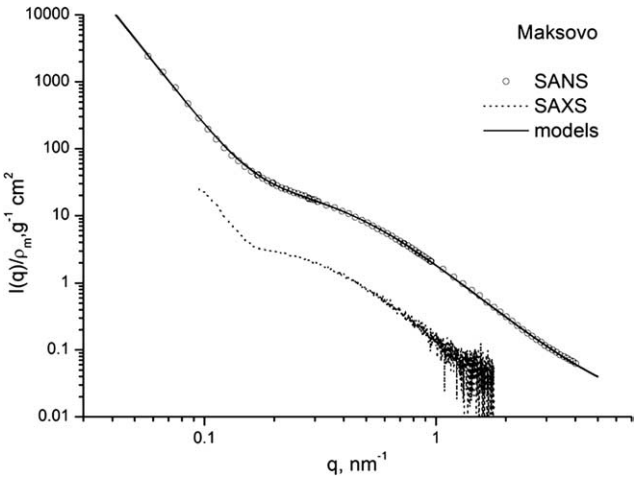

Fig. 2. Experimental SANS and SAXS curves for the Maksovo sample. SAXS curve [15] is referred to the current q-definition and is given in arbitrary units. Fits of the modified Eqs. (6) and (7) to the experimental SANS curve are shown. No significant difference is seen in the resulting model curves (lines). Found parameters are the following. Eq. (6): $B_I = 0.0097$, $P_I = 4.36$, $G_{II} = 26.4\ g^{-1}\ cm^2$, $R_{II} = 4.28$ nm, $B_{II} = 1.87$, $P_{II} = 2.67$, $C = 0.014\ g^{-1}\ cm^2$; Eq. (7): $B_I = 0.0095$, $P_I = 4.35$, $G_{II} = 23.6\ g^{-1}\ cm^2$, $R_{II} = 4.03$ nm, $B_{II} = 1.91$, $P_{II} = 2.68$, $C = 0.015\ g^{-1}\ cm^2$. (dimensions of the B coefficients correspond to the titles of the axes in the graph).

shungites. The scattering curves for different samples differ much, which means that the structural organization of shungite depends strongly on the place where it has been quarried. Despite the difference, still some common features can be distinguished in the scattering curves. Namely, two characteristic levels in each curve are observed showing different types of power-law behavior in the scattering. Estimates of the corresponding exponents (slopes of the curves plotted in the double logarithmic scale in Fig. 1) make it possible to conclude qualitatively about structural peculiarities of the samples at the detected scales. As it was mentioned in the previous Chapter, the characteristic

Table 2
Characteristics of levels detected in the SANS curves

Sample	Level I		Level II	
	Surface dimension	Radius of units (nm)	Mass fractal dimension	Radius of units (nm)
Maksovo	2	>100	2.7	5
Shunga	2	>100	2.2	10
Chebolaksha	2.4	>100	2.7	>20

radius of structural units can be estimated from the q-point where the power-law behavior starts to break (finite size effect) using Eq. (3). One can see that this effect does not take place for level I (small q-values) in all curves, which means that the registered q-interval does not allow one to conclude about the characteristic radius of level I. From the minimal detected q-value a low estimate for corresponding particle radius can be found, which is ~100 nm. This size is associated with large globule units in shungites reported previously [15,16]. For level II (large q-values) the finite-size effect is clearly seen. The results of the estimates of the characteristic radii in this case are given in Table 2.

According to classification (2) one can conclude that level I corresponds to the surface scattering from the large globule units mentioned above. It should be pointed out that the systematic error in determination of the power-law exponent can be large in this case, since the q-interval, where such law is detected, is rather small, and in cases of Maksovo and Shunga just a few points are covered. For this reason, the effect of the scattering of level II on the power-law scattering of level I is significant. Nevertheless, the closeness to the equality $P = 4$ allows one, in accordance with the Porod law, to assume a quite smooth interface producing the scattering and to make some important estimates. The Porod law can be expressed as [24]

$$I(q) = 2\pi n_I(\rho - \bar{\rho})^2 S_I (1/q)^4, \tag{8}$$

where S_I is the characteristic surface of the particles at level I. Comparing (8) with (1) one can see that in the Porod regime

$$B_I = 2\pi n_I(\rho - \bar{\rho})^2 S_I, \tag{9}$$

and, hence, B_I can be used to estimate the size or concentration of the corresponding particles, which is done below. Neglecting the polydispersity effects and assuming for the contrast $(\rho - \bar{\rho})^2$ the difference between carbon ($\rho \sim 7 \times 10^{10}\ cm^{-2}$) and vacuum ($\rho = 0\ cm^{-2}$) such estimates for level I using (9) give the particle concentration of $<10^{13}\ cm^{-3}$ for the lower limit of the characteristic radius (Table 2). This value corresponds to the minimal volume fraction of 4% for the radius of 100 nm. At fixed B_I found in the experiment the volume fraction is proportional to the assumed radius of the particle. Taking into account the high packing density of large shungite units observed in the previous HRTEM experiments [8,12], one can conclude that level I is composed of a small amount of pores of the same radius as the units within packed unit

structure. The inner surface area of these pores calculated directly from (9) is about 0.3 $m^2 g^{-1}$. Comparing this value with the corresponding results of BET (Table 1) one can conclude that the main contribution into the inner surface comes from level II especially in the case of the Maksovo shungite.

Level II reflects the volume organization showing the scattering from fractal clusters of characteristic radii given in Table 2. Only for the Chebolaksha sample the background scattering at level II is significant and determined reliably. It is connected with the incoherent scattering, which is produced mainly by hydrogen and is indicative of higher quantity of hydrogen-containing compounds in this sample (hydrogen content ~1.2 wt%) in comparison with the other two, 0.5 and 0.8 wt% for Shunga and Maksovo, respectively [25]. The detailed treatment of level II according to Eqs. (6), (7) is possible for the Maksovo sample only. In this case the finite-size effect is pronounced, and parameters G_{II} and R_{II} can be determined with a good accuracy. The results of such treatment are shown in Fig. 2. One can see that both Eqs. (7), (8) satisfy well the experimental data and the corresponding fits result in only ~10% difference in the G_{II}, R_{II} parameters. By analogy with level I, using (5) the particle concentration at level II is ~10^{17} cm^{-3}, which, taking the characteristic radius into account (Table 2), results in the volume fraction of <10% for these particles. Taking into account absorption properties of shungites one can assume that the best candidate for the producer of the scattering at level II is also the pore system.

To separate the scattering from the open and closed porosity at both levels the contrast matching was used. As it was mentioned above, for this purpose the deuterated water (D_2O) was added to the samples. After the open pores in shungites had absorbed D_2O, the scattering experiments were repeated. The corresponding changes in the scattering are demonstrated in Fig. 3 for samples from Maksovo and Shunga deposits. These shungites differ much with respect to the ratio between open and closed porosity according to the BET data (Table 1). In fact, the lower curves in Fig. 3 correspond to the situation when open pores in the given samples are filled with heavy water, and, hence, the scattering from the open porosity is almost matched. One can see that significant changes in the scattering take place at both levels for the two samples.

First, the scattering intensity at level I in both samples decreases by a factor of ~100, while its character remains the same. The most probable explanation of this effect is just a change in the contrast. As one can see, there is a small difference in the scattering length densities of carbon and D_2O (see Introduction), which is about 0.7×10^{10} cm^{-2}. It is ten times less than initial difference between carbon and vacuum. Hence, if voids in the samples are filled with heavy water the intensity should decrease by a factor of about 100 due to the squared contrast factor $(\rho - \bar{\rho})^2$. This suggests that all pores in the samples responsible for the scattering at level I should be filled with heavy

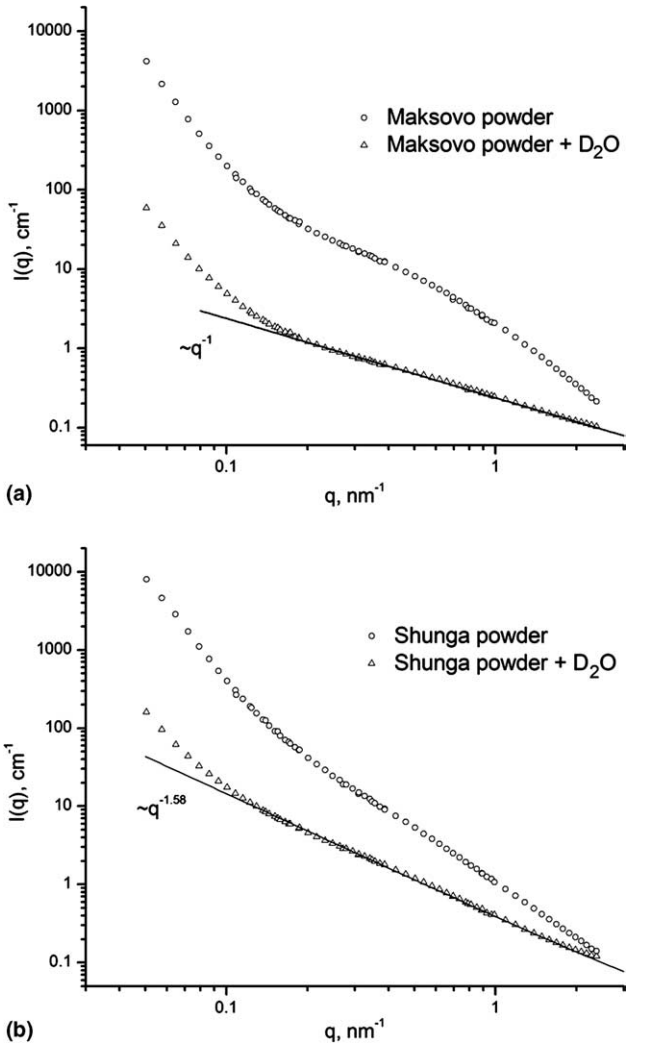

Fig. 3. Comparison of the SANS curves from initial shungite powders and after the adsorption of deuterated water (D_2O). Significant changes at both scattering levels are seen. Solid lines correspond to the scattering of the power-law type (1).

water, which, in its turn, means that if there are large voids in the shungite units ($R > 100$ nm) then they can accept water. Otherwise, a high contrast between the voids and carbon/heavy water bulk would be conserved and such great changes in the absolute values of the scattering at level I would not be observed. This agrees well with the concept of small amounts of unit gaps in the packed structure of large shungite units.

Changes at level II during the D_2O absorption are more significant. They differ in character in comparison with level I. Thus, for the Maksovo shungite the finite-size effect is seen no more, and the exponent in the power-law regime transforms to −1. Changes at level II for the Shunga sample are smaller, which is in accordance with the smaller open porosity in this type of shungites (Table 1). The exponent in the power law decreases down to −1.58, and a weak finite-size effect appears. Since, as it was mentioned above, the scattering from the open pores filled with D_2O decreases by two orders of magnitude, the observed signals

at level II may correspond mainly to the closed pores, which cannot accept D_2O, or to the particles with the scattering length density, which differ greatly from that of carbon and whose effect is small in initial powders because of small concentration. The last variant seems to be unlikely, no such particles were reported in the previous investigations. It is interesting that in the case of the Maksovo sample the curve at level II can be connected with highly elongated particles producing the scattering of power-law type with an exponent -1 (Fig. 3(a)). From the left and right boundary q-values of this regime in the SANS curve one can estimate, according to Eq. (3), the limits for the characteristic length of these particles, $L > 60$ nm, and their cross-sectional radius, $R < 2$ nm, respectively. The concentration of these particles can be estimated for the limits $L = 60$ nm, $R = 2$ nm using the expression for the scattering intensity from highly elongated particles in monodisperse approximation:

$$I(q) = \pi n(\rho - \bar{\rho})^2 S_c^2 L/q, \tag{10}$$

where S_c is the characteristic cross-section area of the particles. From (10) it follows that:

$$B_{II} = \pi n(\rho - \bar{\rho})^2 S_c^2 L. \tag{11}$$

Using the experimental value of B_{II} the last equation gives for n the value of $\sim 10^{15}$ cm^{-3}, which is about 100 times less than that for the open pores at level II in this sample. This value is inverse to the length of the elongated particles. The observed elongated pores can be connected with the peculiarities of the unit packing in the Maksovo sample manifesting a texture organization, i.e., the units are slightly elongated and oriented along one direction in separate blocks (size ~ 4 μm) [14]. This can be clearly seen in electron microscopy images (Fig. 4). As concluded from the SANS measurements, a part of the pores between the units are elongated and closed. They do not show any inner structure and can be considered as homogeneous particles. The shungite from Shunga is quite isotropic, no texture was detected at these levels by electron microscopy. In this sample a significant part of the pores at level II is closed pores, which explains the difference in the ratio between open and closed porosity according to the BET data.

So, it is shown that the open porosity makes a significant contribution into the scattering at level II in shungites. Along with it one can see that the particles responsible for the scattering at level II possess an inner fractal-type structure. It is interesting that the size of units composing such structure is beyond the resolution of the SANS method, which is ~ 1 nm. It follows from the fact that no finite-size effect for them is seen at large q-values at level II. The most probable model of level II is the fractal clusters of small carbon formations with the size of less than 1 nm which are located within large shungite units or in voids between. In particular, they can consist of the minimal structural elements of 0.51 nm detected [11,15] by HRTEM and X-ray diffraction in shungites including the samples studied in the given work. These elements could form and take part in the clusterization under the hydrothermal influence and changing heat–pressure conditions shown in the previous structural investigations [11,14]. A weak connection of some elements, i.e., the possibility of their migration during late development of shungite rocks was ascertained [25].

The number of units in a cluster at level II can be estimated by the relation:

$$N \sim (R_{II}/R_0)^{D_{II}}, \tag{12}$$

where R_0 is the effective radius of the unit. For the Maksovo sample, assuming $R_0 = 0.25$ nm, one obtains $N \sim 1750$ which can be used for calculations of the inner surface area of level II and results in about 130 m^2 g^{-1}. This value is one and a half times less than that obtained in the BET experiments (Table 1). Still, one can consider it as a good agreement of both techniques, since in the current calculations the basic units were assumed to be spherical, which is not true.

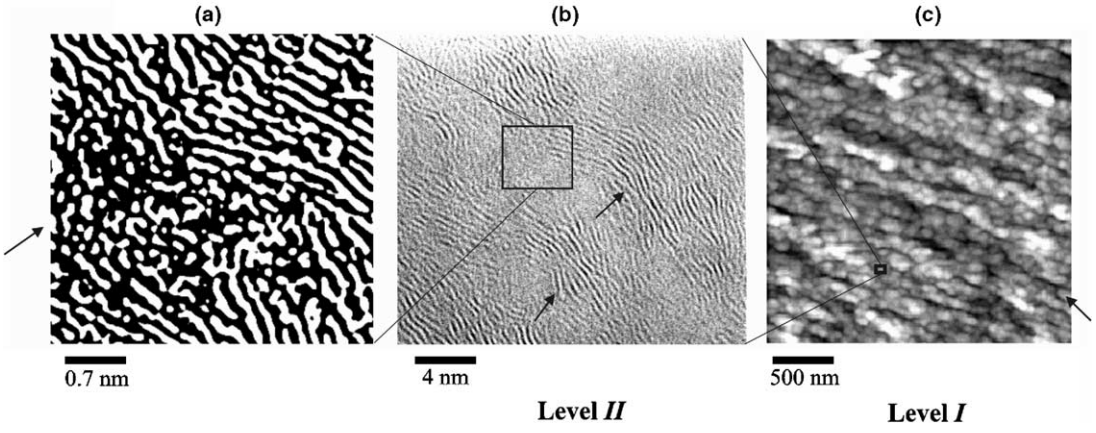

Fig. 4. Different scales in structure of the Maksovo shungite by the data of electron microscopy. (a) Contrasting imprint of the HRTEM image of (b), arrow shows the pore between carbon stacks (basic structural units) filled with non-structured fractal carbon; (b) HRTEM image of packing of basic structural units (after [13]), arrows show BSUs; (c) AFM image of shungite fracture (after [16]), arrow shows a large globule unit. Levels I and II correspond to those observed in SANS experiments. A preferable texture direction at both levels can be seen.

Also, fullerenes (size ~1 nm) whose traces were observed in shungites [8,9] can be mentioned with respect to the possible units of the clusters at level II, as well as some analogs of these clusters in fullerene soots [26] can be found. It is important that vapour and fluid composition used in the preparation of the soots influences much the dimension and structural morphology of the clusters [26].

Summarizing the obtained results one can conclude that the origin of the observed multiscale organization of shungites is connected with the formation of different structural units within them. It is evident from the given SANS data that small nanopores (size ~1 nm) exist in shungites, but their identification is out of the range covered by the technique. The presence of polyaromatic structures (small graphene layers), their imperfect stacking and random orientation of the stacks [11,12] can be responsible for the appearance of the fractal clusters at this scale. The characteristic size of these clusters is associated with that of the basic structural units (BSU) in shungites (less than 10 nm), first proposed as coherent domains detected by X-ray diffraction and seen as stacks of layers by HRTEM [11]. Later, the analysis of the HRTEM data and electron nanodiffraction patterns resulted in conclusions that BSU are three-dimensional closed layered structures or fractions of such curved structures regarded as short bent stacks (or fractions of closed shells) [12,13], which are illustrated in Fig. 4 for the Maksovo shungite. According to the SANS data level II reflects the organization of the pores inside and between aggregates of BSU. These aggregates compose the large globule units of size >100 nm detected by AFM [15,16], which are tightly packed, however, some fraction of open pores (<10 vol%) within this structure exists and produces SANS signal corresponding to level I (Fig. 4).

4. Conclusions

Our SANS study reveals that shungites possess a complex pore organization at a nanoscale of 1–100 nm. Despite the fact that the morphology of the shungites depends on the natural factors (temperature, pressure and composition of fluids) taken place at a deposit two structural levels can be distinguished for all samples. The first level (characteristic particle radius >100 nm) corresponds to the so-called large shungite units. The most probable producer of the scattering at this scale is a small fraction (<10 vol%) of pores as a result of gaps in the high packing of these shungite units. Smaller particles (characteristic radius of ~10 nm) at the second structural level are the mixture of open and closed pores inside or between large shungite units. Their size is associated with that of the basic structural units of shungites. The effect of the ratio between open and closed porosity observed in the SANS contrast variation experiments correlates with the BET data. The shape of these pores can be affected by the sample texture, in particular, resulting in their elongation. The pores at the second level are filled with fractal structures of particles with a size beyond the resolution of the SANS method, ~1 nm. These particles can be small bent graphene stacks (size 0.51 nm) or fullerenes (size 1 nm) reported earlier for shungites.

Acknowledgment

The work has been performed with the support of ISTC, project 2769.

References

[1] Buseck PR, Galdobina LP, Kovalevski VV, Rozhkova NN, Valley JW, Zaidenberg AZ. Shungites: the C-rich rocks of Karelia, Russia. Can Mineral 1997;35(6):1363–78.
[2] Grigorieva EN, Rozhkova NN. Shungite carbon behaviour in the modelling reactions of coal thermal decomposition. J Appl Chem 2000;73(4):600–5.
[3] Zaidenberg AZ. Shungite influence on the water. In: Extended abstracts 23d biennial conference on carbon, Pennstate, 1997. USA: American Carbon Society; 1997. p. 118–9.
[4] Rozhkova NN. Shungite – a carbon-mineral filler for polymeric composite materials. Compos Interface 2001;8(3,4):307–12.
[5] Rozhkova NN, Iordache I, Bondar AM, Pasuk I, Rand B. Natural and synthetic ceramics with shungite carbon. In: Extended abstracts conference on Carbon, Beijing, 2002. p. 73– 5(CD).
[6] Solovov VK, Tupolev AG, Zaidenberg AZ, Zverev AA, Kalinin YuK. Shungite in radio screening composites. In: Fridlyander IN, Kostikov VI, editors. MICC-90 Moscow international composites conference, Moscow, 1990. Kluwer Academic Publishers; 1991. p. 1343–7.
[7] Tuktamushev ISh, Tuktamushev II, Kalinin YuK, Seleznev AN, Gnedin YuF. Properties of Karelian shungite rocks and perspectives of their future using. Fossil Fuels Chem 2001;4:80–8.
[8] Buseck PR, Tsipursky SJ, Hettich R. Fullerenes from geological environment. Science 1992;257:215–7.
[9] Rozhkova NN, Andrievsky GV. Fullerenes in shungite carbon. In: Pilipenko VA, Poklonski NA, editors. Fullerenes and fullerene-like structures. Minsk: Bel. St. University; 2000. p. 63–8 [in Russian].
[10] Andrievsky GV, Kosevich MV, Vovk OM, Shelkovsky VS, Vashechenko LA. On the production of an aqueous colloidal solution of fullerenes. J Chem Soc Chem Commun 1995;12:1281–2.
[11] Jehlička J, Rouzaud J-N. Glass-like carbon: new type of natural carbonaceous matter from Precambrian rocks. Carbon 1992;30:1133–4.
[12] Kovalevski VV, Buseck PR, Cowley JM. Comparison of carbon in shungite rocks to other natural carbons: an X-ray and TEM study. Carbon 2001;39(2):243–56.
[13] Kovalevski VV, Prikhodko AV, Buseck PR. Diamagnetism of natural fullerene-like carbon. Carbon 2005;43(2):401–5.
[14] Kovalevski VV, Rozhkova NN, Zaidenberg AZ, Yermolin AN. Fullerene-like structures in shungite and their physical properties. Mol Mat 1994;4:77–80.
[15] Rozhkova NN, Golubev EA, Siklitsky VI, Baidakova MV. Shungite as aggregates of carbon nanoparticles. In: Extended abstracts, Conference on carbon, Oviedo; 2003. p. 104–7(CD).
[16] Rozhkova NN, Golubev EA, Siklitski VI, Baidakova MV. Structural organization of fullerene-like shungite carbon. In: Vityaz' PA et al., editors. Minsk: UP"Tehnoprint; 2005. p. 100–7 [in Russian].
[17] Rozhkova NN, Owczarek M, Mianowski A. Activation of shungite carbon. In: Vityaz' PA et al., editors. Fullerenes and fullerene containing materials. Minsk: UP"Tehnoprint; 2002. p. 27–32.
[18] Ostanevich YuM. Time-of-flight small-angle spectrometers on pulsed neutron sources. Macromol Chem Macromol Symp 1988;15:91–103.
[19] Serdyuk IN. Small-angle neutron instrument YuMO (JINR, Dubna): some new results and perspectives. Physica B 1997;234–236:892–4.
[20] Jacrot B. Study of biological structures by neutron-scattering from solution. Rep Prog Phys 1976;39:911–53.

[21] Zhao J, Meerwinck W, Niinkoski T, Rijillart A, Schmitt M, Willumaeit R, et al. The polarized target station at GKSS. Nucl Instr Meth A 1995;356:133–7.
[22] Schmidt PW. Some fundamental concepts and techniques useful in small-angle scattering studies of disordered solids. In: Modern aspects of small-angle scattering. Netherlands: Kluwer Academic Publishers; 1995. p. 1–56.
[23] Beaucage G. Small-angle scattering from polymeric mass fractals of arbitrary mass-fractal dimension. J Appl Crystallogr 1996;29:134–49.
[24] Feigin LA, Svergun DI. Structure analysis by small-angle X-ray and neutron scattering. New York: Plenum Press; 1987.
[25] Rozhkova NN, Zaidenberg AZ, Golubev AI. Distributuion of trace elements in the carbon-rich shungite rocks of Karelia. In: Challenges to chemical geology, Refereed papers from MAEGS-10, Prague; 1998. p. 137–44.
[26] Gorelik OP, Dyuzhev GA, Novikov DV, Oichenko VM, Fursei GN. Cluster structure of the particles of fullerene soot and fullerene C60 powder. Zhur Techn Phys 2000;70(11):118–25 [in Russian].